

UCC Library and UCC researchers have made this item openly available. Please [let us know](#) how this has helped you. Thanks!

Title	The optical response of nanostructured surfaces and the composite diffracted evanescent wave model
Author(s)	Gay, G.; Alloschery, O.; Viaris de Lesegno, B.; O'Dwyer, Colm; Weiner, J.; Lezec, H. J.
Publication date	2006-03-26
Original citation	Gay, G., Alloschery, O., de Lesegno, B. V., O'Dwyer, C., Weiner, J. and Lezec, H.J. (2006) 'The optical response of nanostructured surfaces and the composite diffracted evanescent wave model'. Nature Physics, 2(4), pp. 262-267. http://dx.doi.org/10.1038/nphys264
Type of publication	Article (peer-reviewed)
Link to publisher's version	http://dx.doi.org/10.1038/nphys264 Access to the full text of the published version may require a subscription.
Rights	© 2006 Nature Publishing Group.
Item downloaded from	http://hdl.handle.net/10468/2839

Downloaded on 2019-04-22T23:57:05Z

Optical Response of Nanostructured Surfaces: Experimental Investigation of the Composite Diffracted Evanescent Wave Model

G. Gay, O. Alloschery, B. Viaris de Lesegno,* C. O'Dwyer,† and J. Weiner
IRSAMC/LCAR, Université Paul Sabatier, 118 route de Narbonne, 31062 Toulouse, France

H. J. Lezec

*Thomas J. Watson Laboratories of Applied Physics,
California Institute of Technology, Pasadena, California 91125 USA and
Centre National de la Recherche Scientifique, 3, rue Michel-Ange, 75794 Paris cedex 16, France*

(Dated: February 14, 2006)

Investigations of the optical response of subwavelength structure arrays milled into thin metal films has revealed surprising phenomena including reports of unexpectedly high transmission of light. Many studies have interpreted the optical coupling to the surface in terms of the resonant excitation of surface plasmon polaritons (SPPs), but other approaches involving composite diffraction of surface evanescent waves (CDEW) have also been proposed. We present here a series of measurements on very simple one-dimensional (1-D) subwavelength structures with the aim of testing key properties of the surface waves and comparing them to the CDEW and SPP models.

I. INTRODUCTION

Initial reports of dramatically enhanced transmission through arrays of subwavelength holes in thin films and membranes [1–3] have focused attention on the physics underlying this surprising optical response. Since the early experiments were carried out on metal films, surface plasmon polaritons [4, 5] were invoked to explain the anomalously high transmission and to suggest new types of photonic devices [5]. Other interpretations based on “dynamical diffraction” in periodic slit and hole arrays [6, 7] or various kinds of resonant cavity modes in 1-D slits and slit arrays [8, 9] have also been proposed. Reassessment of the earlier data by new numerical studies [10] and new measurements [11] have prompted a sharp downward revision of the enhanced transmission factor from $\simeq 1000$ to $\simeq 10$ and have motivated the development of a new model of surface wave excitation termed the composite diffracted evanescent wave (CDEW) model [11]. This model builds a composite surface wave from the large distribution of diffracted evanescent modes (the inhomogeneous modes of the “angular spectrum representation” of wave fields [12]) generated by a subwavelength feature such as a hole, slit, or groove when subjected to an external source of propagating wave excitation. The CDEW model predicts three specific surface wave properties. First, the surface wave is a composite or “wave packet” of modes each evanescent in the direction normal to the surface. The surface wave packet exhibits well-defined nodal positions spaced by a characteristic wavelength, λ_{surf} ; second, the appearance of the first node at a distance of $\lambda_{\text{surf}}/2$ from the subwavelength launch site (essentially a phase delay of $\pi/2$ with respect to the E-field of the external driving source); and third, an amplitude decreasing inversely with distance from the launch site. We present here the results of a series of experiments on very simple 1-D subwavelength surface structures designed to investigate these predictions and thus assess the validity of the model.

II. SUMMARY OF THE CDEW MODEL

The essential elements of the CDEW model can best be summarised with reference to Fig. 1. It is based on a solution to the 2-D Helmholtz equation in the near field and subject to the slab-like boundary conditions of a slit in an opaque screen. The basic expression describing the scalar wave is

$$[\nabla^2 + k^2] E(x, z) = 0 \quad (1)$$

with $\nabla^2 = \partial^2/\partial x^2 + \partial^2/\partial z^2$, $k = 2\pi/\lambda$ and $E(x, z)$ the amplitude of the wave propagating in the x, z directions. Kowarz [13] has written down the solution to this equation for the case of an incident plane wave propagating in air

*Present address: Laboratoire Aimé Cotton, Campus d’Orsay, 91405 Orsay, France

†Present address: Photonic Nanostructures Group Tyndall National Institute, Lee Maltings, Cork, IRELAND

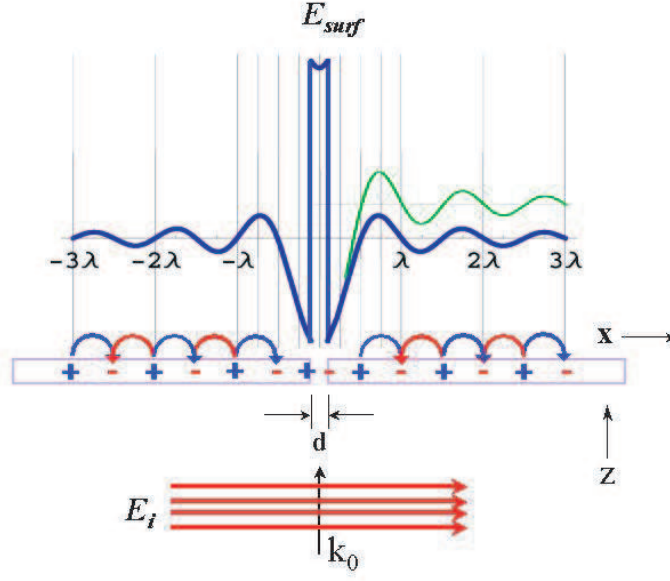


FIG. 1: Essential elements of the CDEW model. The incoming plane wave E_i with $k_0 = 2\pi/\lambda_0$ in air ($n = 1$) is linearly polarised parallel to the plane of the structure and perpendicular to the slit of subwavelength width d . A fraction of the incoming light E_{surf} forms the composite diffracted wave in the $\pm x$ directions, and the blue trace (displaced above the surface for clarity) shows E_{surf} . The alternating blue and red loops indicate the field lines induced by the CDEW near the surface of the silver film. The green trace (offset above the blue trace for clarity) shows the cosine representation of the CDEW expressed by Eq. 4 and closely approximating Eq. 2a for $|x| \geq 3/4\lambda$. The wavelength $\lambda_{surf} = \lambda_0/n_{surf}$ where n_{surf} is the surface index of refraction.

($n = 1$) with amplitude E_i and propagation vector k_0 impinging on a slit of width d in an opaque screen. Specifying the coordinates as shown in Fig. 1, the field solution E_{ev} for the modes evanescent in z at the $z = 0$ boundary is

$$E_{ev}(x, z = 0) = -\frac{E_i}{\pi} \left\{ \text{Si} \left[k \left(x + \frac{d}{2} \right) \right] - \text{Si} \left[k \left(x - \frac{d}{2} \right) \right] \right\} \quad \text{for } |x| > d/2 \quad (2a)$$

$$= \frac{E_i}{\pi} \left\{ \pi - \text{Si} \left[k \left(x + \frac{d}{2} \right) \right] + \text{Si} \left[k \left(x - \frac{d}{2} \right) \right] \right\} \quad \text{for } |x| \leq d/2 \quad \text{with } \text{Si}(\alpha) \equiv \int_0^\alpha \frac{\sin(t)}{t} dt \quad (2b)$$

The k_z evanescent modes are determined by a conservation-of-energy criterion,

$$k_z = \sqrt{k_0^2 - k_x^2} \quad k_x > k_0 \quad (3)$$

The form of the inhomogeneous or evanescent field on the $z = 0$ boundary is shown in Fig. 1. At transverse displacements from the slit $|x| > d/2$, the evanescent component of the field at the surface $E_{ev}(x, z = 0)$ can be represented to good approximation by the expression

$$E_{ev} \simeq \frac{E_i d}{\pi x} \cos(k_{surf} x + \pi/2) \quad (4)$$

that describes a damped wave with amplitude decreasing as the inverse of the distance from the launching edge of the slit, a phase shift $\pi/2$ with respect to the propagating plane wave at the midpoint of the slit and a wave vector $k_{surf} = 2\pi/\lambda_{surf}$. The wavelength of the CDEW on the surface $\lambda_{surf} = \lambda_0/n_{surf}$ where n_{surf} is the surface index of refraction (empirically, $n_{surf} \simeq 1.04$). This surface wave is actually a composite superposition of k_x modes evanescent in z , with $|k_x| > k_0$ and directed along the $\pm x$ axes.

$$E_{ev}(x, z) = \frac{E_i}{\pi} \int_{\pm k_0}^{\pm\infty} dk_x \frac{\sin(k_x d/2)}{k_x} \exp(ik_x x) \exp(-k_z z) \quad (5)$$

Equation 5 generalises the expressions of Eqs. 2a, 2b to include the evanescent components above the $z = 0$ plane. When the composite evanescent wave encounters a surface discontinuity (a slit for example), a fraction of the surface wave is reconverted to a distribution of “homogeneous” or propagating modes $|\mathbf{k}| = 2\pi/\lambda_0$ at the site of the slit. In a

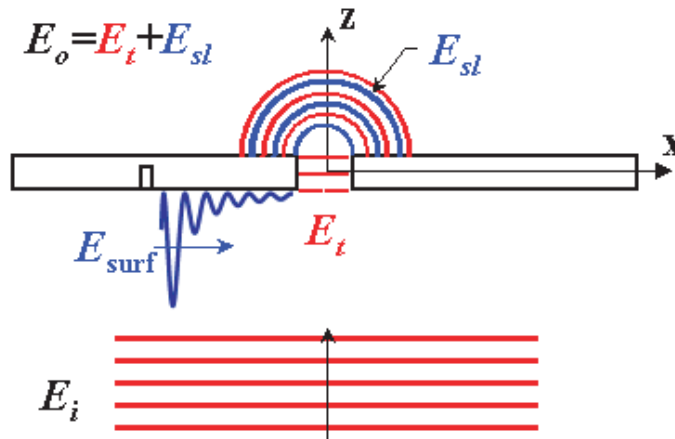


FIG. 2: The incoming plane wave E_i impinges on the subwavelength slit (or hole) and a groove milled on the input side. The evanescent E_{surf} wave originates on the surface at a slit-groove distance x_{sg} and is indicated in blue. In the model proposed in [11] CDEWs travel along the surface toward the slit where they reconvert to a propagating field E_{sl} and interfere with E_t , the propagating field directly transmitted through the slit or hole. The superposed output field $E_o = E_t + E_{sl}$ propagates into the $z \geq 0$ half-space and the intensity of the interference figure $I(\theta)$ is detected in the far field.

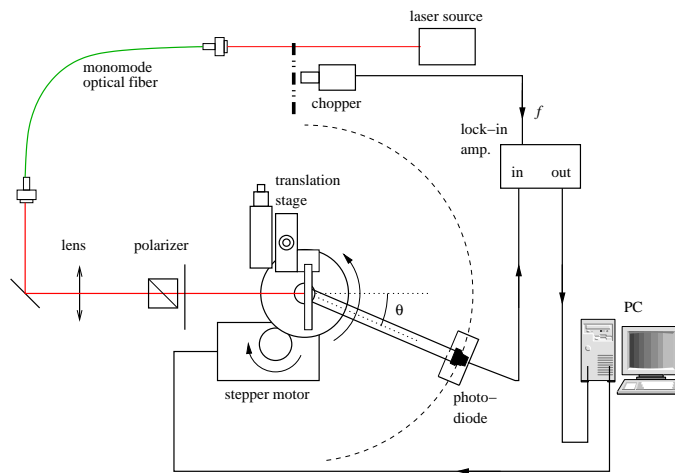


FIG. 3: Goniometer setup for measuring far-field light intensity and angular distributions. A stabilised single mode CW diode laser, locked to a wavelength of 852 nm and modulated at 850 Hz by a chopper wheel, is injected into a single-mode fibre and focused onto the nanostructures mounted in a x-y translation stage as shown. A stepper motor drives the goniometer arm, and the chopped light intensity detected by the photodiode is fed to a lock-in amplifier. Output from the lock-in is registered by the PC that also drives the stepper motor. For the input-side experiments described here the detector was always positioned at $\theta = 0^\circ$.

practical experiment, any real planar structure has two surfaces: an “input side” in the half-space $z < 0$, containing the incoming plane wave, and an “output side” in the half-space $z \geq 0$, containing the far-field propagating modes issuing from the output surface and a photodetector. Experiments can be carried out by fabricating subwavelength grooves on the input side, the output side or both. The measurements reported here concern only the input-side experiments (Fig. 2). Results for output-side experiments will be reported later.

III. MEASUREMENTS AND RESULTS

Measurements of the optical response of the slit-groove and hole-groove structures were carried out using a home-built goniometer shown in Fig. 3, details of which are described in the caption of Fig. 3 and in the Methods section. We have carried out a series of measurements on simple 1-D structures to test the “signature” predictions of the CDEW model, *viz.* (1) a composite surface wave expressed by Eq. 5 and approximately represented by a damped

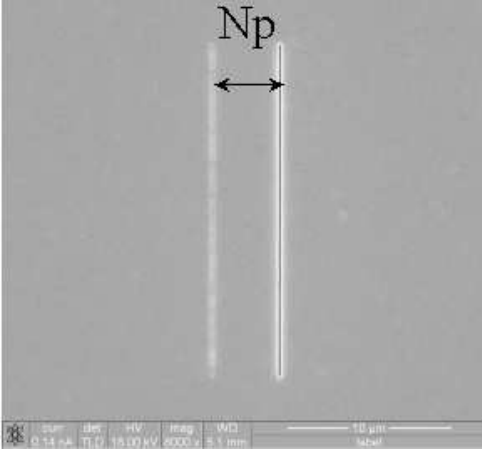


FIG. 4: Scanning electron microscope (SEM) image of one of the series of single-slit, single-groove structures FIB milled into a 400 nm thick silver layer deposited on flat quartz microscope slides 1 mm thick. The width of both the slit and the groove is 100 nm, the height $20\mu\text{m}$ and the groove depth ~ 100 nm. The distance Np is the pitch increment $p = 104$ nm multiplied by the number of increments N .

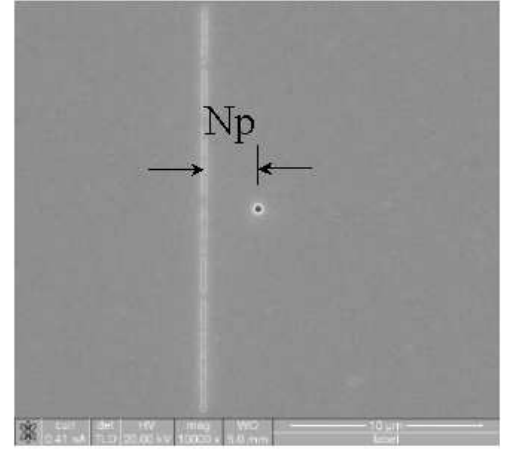


FIG. 5: SEM image of one of the series of single-groove, single-hole structures fabricated similarly to the single-groove, single-slit structures of Fig. 4. The silver layer for the groove-hole structures is 260 nm thick, the width and depth of the groove is 100 nm and 70 nm respectively, and the diameter of the hole is 300 nm. The distance Np is the pitch increment $p = 104$ nm multiplied by the number of increments N .

wave, Eq. 4; (2) a phase shift of $\pi/2$ between the CDEW and the driving source plane wave and (3) a wave amplitude that decreases inversely with distance from the launching groove. Figures 4, 5 show one of the series of structures consisting of one slit and one groove and one hole and one groove, respectively. The slit-groove distance x_{sg} or hole-groove distance x_{hg} is indicated as Np where p is the basic unit of distance increment, the “pitch,” and N is the number of increments. The pitch p was taken to be 104 nm, approximately one-eighth the wavelength of the surface wave and N was varied from 4 to 59. Structural details of these devices are described in the captions of Figs. 4, 5 and in the Methods section. The slit(hole)-groove structures were mounted facing the input side and exposed to plane-wave radiation from the focused TEM_{00} laser source. Measurements of light intensity on the output side in the far field, 200 mm from the plane of the structures, were carried out on the slit-groove structures using the goniometer setup described in the Methods section. The results are shown in Figs. 6, 7. They show an oscillatory fringe pattern with amplitude damping out to a distance of $\simeq 3 - 4 \mu\text{m}$ and maintaining an essentially constant amplitude from that point out to the distance limit of the measurements. As indicated in Fig. 2, the fringe pattern results from interference between the mode directly propagating through the slit (hole) at the input side E_t and a surface wave originating from the single-groove structures E_{surf} . The wave E_{surf} is reconverted to a propagating mode at the slit or hole, and it is this propagating mode that interferes with E_t . The frequency and phase of the interference pattern is a function of the slit (hole)-groove optical path and any intrinsic phase shift of the surface wave itself. The normalised intensity I/I_0 of the superposition term is given by

$$\frac{I}{I_0} = 1 + \eta_i^2 + 2\eta_i \cos \gamma_i \quad \text{with} \quad \eta_i = \frac{\alpha\beta}{\delta} \quad (6)$$

where $\alpha = E_{\text{surf}}/E_i$ is the fractional amplitude of the surface wave launched from the incoming field E_i at the groove site, and β is the further fraction of this surface wave reconverted to a propagating wave in the slit, $E_{sl} = \beta E_{\text{surf}} = \beta\alpha E_i$. The fractional amplitude of the directly transmitted component E_t is δ and the phase difference γ_i between E_t and E_{sl} is the sum of two terms,

$$\gamma_i = k_{\text{surf}}x_{sg(hg)} + \varphi_{\text{int}} \quad (7)$$

The first term $k_{\text{surf}}x_{sg(hg)}$ is the phase accumulated by the surface wave propagating from the groove to the slit (hole) and the second term φ_{int} is any phase shift intrinsic to the surface wave. The term φ_{int} includes the “signature” shift of the CDEW plus any phase shift associated with the groove width and depth. Figures 6, 7 present a direct measure of the normalised amplitude damping with distance, $\eta_i = \eta_i(x)$ and the period and phase of the oscillations, from which the wavelength λ_{surf} of the surface wave, the phase φ_{int} , and the effective surface index of refraction n_{surf} can be determined. Analysis of the frequency spectrum of the fringe pattern for the slit(hole) structures results in the determination of a surface wavelength $\lambda_{\text{surf}} = 819(811) \pm 8$ nm and an effective surface index of refraction

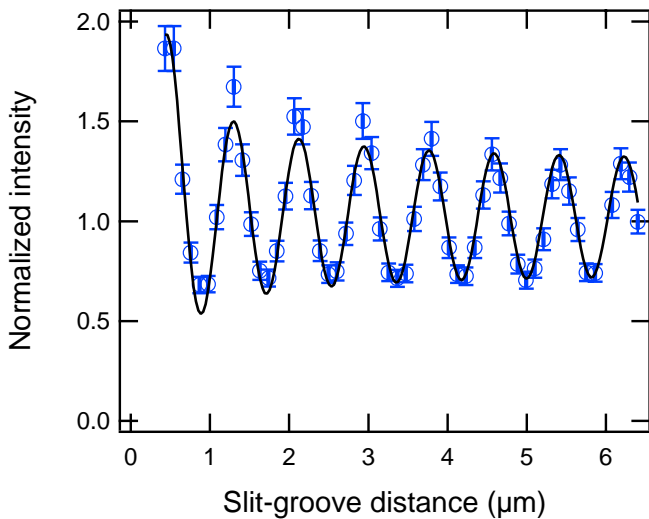


FIG. 6: Normalised far-field intensity I/I_0 as a function of slit-groove distance x_{sg} for series of single-slit, single-groove structures mounted facing the input side with respect to plane wave excitation. Points are the measured data through which the solid line, Eq. 8a, is fitted with parameters $\mu_{sl} = 0.13 \pm 0.01$, $\kappa_{sl} = 0.12 \pm 0.01 \mu\text{m}$ and $\varphi_{\text{int}}^{sl} = 0.81 \pm 0.02\pi$. Error bars were determined from variations in the measured intensities of the six nominally identical naked slits (no flanking groove) used for normalisation of each measurement. Analysis of the frequency spectrum of the fringe pattern for the slit-groove structures results in the determination of a surface wavelength $\lambda_{\text{surf}} = 819 \pm 8 \text{ nm}$ and an effective surface index of refraction $n_{\text{surf}} = 1.04 \pm 0.01$.

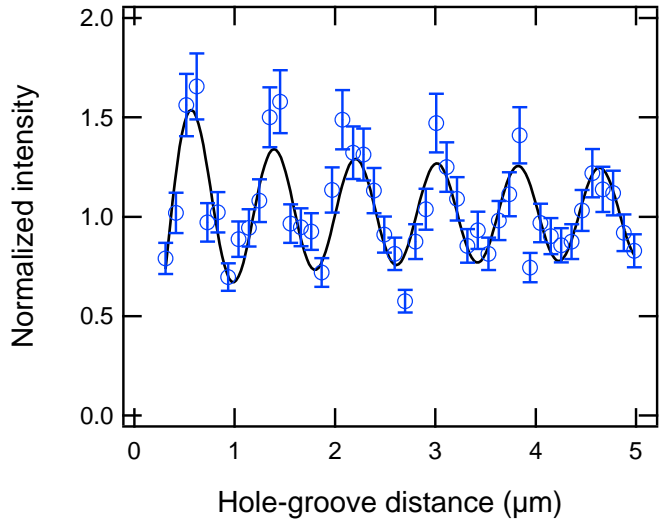


FIG. 7: Normalised far-field intensity I/I_0 as a function of hole-groove distance x_{hg} for series of single-hole, single-groove structures mounted facing the input side with respect to plane-wave excitation. Points are measured data through which the solid line, Eq. 8b, is fitted with parameters $\mu_{hl} = 0.10 \pm 0.02$, $\kappa_{hl} = 0.08 \pm 0.03 \mu\text{m}$, and $\varphi_{\text{int}}^{hl} = 0.55 \pm 0.05\pi$. Error bars were determined from variations in the measured intensities of the six nominally identical naked holes (no flanking groove) used for normalisation of each measurement. Analysis of the frequency spectrum of the fringe pattern for the hole-groove structures results in the determination of a surface wavelength $\lambda_{\text{surf}} = 811 \pm 8 \text{ nm}$ and an effective surface index of refraction $n_{\text{surf}} = 1.05 \pm 0.01$.

$n_{\text{surf}} = 1.04(1.05) \pm 0.01$. The amplitude η_i of the oscillatory term depends on the slit(hole)-groove distance, and Figs. 6, 7 show that η_i falls off with increasing distance. This fall-off is fit to an expression with two terms: an inverse distance dependence term plus a constant term.

$$\eta_i^{sl}(x_{sg}) \cos(\gamma_i) = \left(\frac{\kappa_{sl}}{x_{sg}} + \mu_{sl} \right) \cos(k_{\text{surf}} x_{sg} + \varphi_{\text{int}}^{sl}) \quad (8a)$$

$$\eta_i^{hl}(x_{hg}) \cos(\gamma_i) = \left(\frac{\kappa_{hl}}{x_{hg}} + \mu_{hl} \right) \cos(k_{\text{surf}} x_{hg} + \varphi_{\text{int}}^{hl}) \quad (8b)$$

The best-fit values for μ, κ, φ are indicated in the captions of Figs. 6, 7 and in Table I for slit and hole structures, respectively. The subscript i and superscripts sl, hl on η refer to input-side, slit and hole measurements, respectively.

IV. DISCUSSIONS AND CONCLUSIONS

The measured interference fringes on slit(hole) structures exhibit the presence of a surface wave with wavelength $819(811) \pm 8 \text{ nm}$ and therefore a surface index of refraction $n_{\text{surf}} = 1.04(1.05) \pm 0.01$. The amplitude behavior of these fringes is also similar. Both the slit-groove and hole-groove structures exhibit an initial amplitude fall-off with increasing distance, damping to an essentially constant amplitude at a distance $\simeq 6 \mu\text{m}$. This behavior is fit to the expressions in Eqs. 8a, 8b. The fitting procedure is a linear regression varying the relative contributions of the constant and decaying amplitude terms, $\mu_{sl(hl)}$ and $\kappa_{sl(hl)}$ and the intrinsic phase shift $\varphi_{\text{int}}^{sl(hl)}$. The results are summarized in Table I.

How do these results compare to CDEW or SPP models? In the CDEW picture, the groove launches a surface wave on the input side of the silver film that is detected by interference with the directly transmitted wave through the hole or slit, in the far field, on the output side of the structure. The amplitude of this surface wave is predicted to damp as the inverse distance between the groove and the slit or hole. Figures 6, 7 show an initial decrease in amplitude

TABLE I: Fit parameters and measured n_s for slit and hole structures. Error bars were determined from variations in the measured intensities of the six nominally identical naked slits and holes (no flanking groove) used for normalisation of each measurement in Figs. 6, 7.

parameter	slit structure	hole structure	SPP model
n_{surf}	1.04 ± 0.01	1.05 ± 0.01	1.015
$\lambda_{\text{surf}}(\text{nm})$	819 ± 8	811 ± 8	844
μ	0.13 ± 0.01	0.13 ± 0.02	
$\kappa(\mu\text{m})$	0.12 ± 0.01	0.020 ± 0.020	
$\varphi_{\text{int}}(\pi)$	0.81 ± 0.02	0.55 ± 0.05	

TABLE II: Surface plasmon parameters

Reference	ϵ'_{Ag}	ϵ''_{Ag}	n_{sp}	$L_{\text{abs}}(\mu\text{m})$	$L_{\text{scat}}(\mu\text{m})$	$L_{\text{rad}}(\mu\text{m})$
^a	-33.27	1.31	1.0154	109	2.56×10^4	5.00×10^4
[14]	-34.	0.46	1.015	326	2.6×10^4	5.0×10^4
[15]	-32.4	1.74	1.0158	78.0	2.51×10^4	2.68×10^4

^aMeasurements on silver films used in these experiments carried out at Caltech on a Sentech SE850 ellipsometer, 05 September 2005.

with increasing distance out to about $3 - 4 \mu\text{m}$, but that the amplitude thereafter remains essentially constant. The solid curves in Figs. 6, 7 fit this amplitude decrease to an inverse distance dependence (Eqs. 8a, 8b). However, the damping might also plausibly fit an exponential decrease which would be expected from surface plasmon dissipative processes such as absorption by the silver film or scattering due to surface roughness. In order to check this possibility we have measured the properties of the silver films used in these studies. Table II summarises these properties and compares them to previously reported measurements [14, 15]. The dielectric constant at 852 nm $\epsilon_{\text{Ag}} = \epsilon'_{\text{Ag}} + i\epsilon''_{\text{Ag}}$ was measured by ellipsometry and surface roughness parameters determined by atomic force microscopy (AFM). The root-mean-square (rms) height of the films was measured to be $\delta = 1.29 \text{ nm}$ and the correlation length $\sigma = 154.3 \text{ nm}$. From the imaginary term of the dielectric constant ϵ''_{Ag} and the parameters δ, σ the expected propagation lengths of surface plasmons against absorption, surface scattering, and reradiation, $L_{\text{ams}}, L_{\text{scat}}, L_{\text{rad}}$, can be calculated [4]. It is clear from columns 5-7 of Table II that these loss processes cannot account for the observed damping within $3 \mu\text{m}$ of hole-groove distance.

The constant amplitude beyond $\sim 3 - 4 \mu\text{m}$ is consistent with a persistent surface wave. Indeed we have recorded measurements (not presented here) of the surface wave persisting at least to $\simeq 30 \mu\text{m}$ slit-groove distance. It is important to emphasise, however, that λ_{surf} and n_{surf} deviate significantly for those expected for a pure SPP on a plane silver surface. Interferometry measurements of the surface waves on “output side” slit-groove structures (not reported here) confirm the value of n_{surf} in Table I, and we believe that conventional, infinite-plane SPP theory [4] is not adequate to explain these results. We note that persistent surface waves over $\sim 10 \mu\text{m}$ distances have also been reported in a double slit experiment [16] and interpreted as SPPs [17].

As indicated in Table I, intrinsic phase for the slit-groove and hole-groove structures respectively are $\varphi_{\text{int}}^{\text{sl}} = 0.81 \pi$ and $\varphi_{\text{int}}^{\text{hl}} = 0.55 \pi$. Although one contribution to these phase shifts may be the CDEW “signature” phase shift of $\pi/2$, it is known from earlier studies that the specific form (width and depth) of the grooves themselves, can introduce phase shifts into the scattered wave [9]. We have determined the nature of these groove-induced phase shifts and resonances by measuring interference fringes arising from surface waves launched on the “output-side” of slit-groove structures. These results, that will be reported in a subsequent publication, support the existence of an intrinsic phase shift close to $\pi/2$.

The interpretation that emerges from these results is that the subwavelength groove originates persistent, long-range surface waves by a two-step process: (1) the incoming TM polarised plane wave scatters from the groove and generates in its immediate vicinity on the surface a broad, CDEW-like distribution of diffracted evanescent waves, and (2) this broad-band local surface “emitter” excites, within a distance of $\simeq 3 - 4 \mu\text{m}$, a long-range surface wave response. The near-term rapid amplitude decrease in the interference fringes of Figs. 6, 7 is evidence of this evanescent surface wave diffraction very near the groove. Persistent amplitude out to tens of microns is evidence for some kind of surface wave guided mode. It is significant to note that the wavelength and phase of the interference fringes do not shift over the entire range of the measurements. The initial diffracted surface wave components extend over a broad range of evanescent modes, $k_x > k_0$, including the conventional k_{SPP} . Therefore it is to be expected that the local surface wave emitter excites this surface mode. We emphasise, however, that our measurements show that the wavelength of this persistent wave does not correspond to k_{SPP} and that, when the phase lag associated the groove

itself is taken into account, the intrinsic phase of the surface wave with respect to the directly transmitted wave is close to $\pi/2$. The disaccord between λ_{SPP} and λ_{surf} is for the present a matter of speculation. Perhaps plasmon “leaky waves” [21] that transport energy very slowly away from the surface contribute to the spectrum of long-range surface excitation resulting in an effective wavelength shift; or perhaps, despite our ellipsometry measurements, the surface index of refraction of the metal film is slightly modified by some uncontrolled chemical or material process [22]. At a more practical level, these results indicate that it might be much easier to couple to surface guided waves than was previously thought. Conventional wisdom asserts that because the SPP lies to the right of the “light line” on the metal surface dispersion curve, a grating or prism is needed to achieve efficient optical coupling [4]. A simple abrupt discontinuity in the surface, such as a slit or groove, appears to serve as an efficient coupler. Further studies are needed to understand the properties of the generated long-range persistent wave and to optimise the efficiency of this groove-coupling process.

V. METHODS

A. Structure fabrication

The structures consist of a single subwavelength slit or hole flanked by one subwavelength groove. The grooves have a width of 100 nm and a nominal depth of 100 nm for the slit-groove structures and 70 nm for the hole-groove structures. The slit-groove distance (x_{sg}) or hole-groove distance (x_{hg}) is systematically incremented in the fabrication process. The subwavelength structures are fabricated by focused ion beam (FIB) milling (FEI Nova-600 Dual-Beam system, Ga^+ ions, 30keV) into a layer of silver evaporated onto flat fused silica microscope slides. A low beam current (50 pA) was used in order to achieve surface features defined with a lateral precision on the order of 10 nm and characterised by near-vertical sidewalls and a minimal amount of edge rounding. Since it enables delivery of a variable ion dose to each pixel of the writing field, FIB milling conveniently allows the multiple-depth topography characteristic of the present devices to be formed in a single, self-aligned step. A 2-D matrix of structures is milled into the silver layer. Each matrix consists of 63 structures, nine columns, separated by 1.5 mm, and seven rows, separated by 2 mm. The first column contains only the slit with no flanking grooves. Light transmission through the slits in this column is used to normalise the transmission in the remaining columns. Variations in transmission through each of the elements in the “slits only” column provide a measure of the uniformity of the FIB fabrication process. Each entire matrix of structures is flanked on one side by a small round hole and on the other by a line grating for absolute reference positioning and angular alignment of the structure matrix with respect to the input laser beam. The square microscope slides themselves, commercially available from SPI Supplies, are 25 mm on a side and 1 mm thick.

B. Measurement Setup

Details of the experimental setup are as follows. Output from a diode laser source, temperature stabilised and frequency-locked to $^2\text{S}_{1/2}(\text{F} = 4) \rightarrow ^2\text{P}_{3/2}(\text{F} = 4, 5)$ crossover feature in a Cs saturated absorption cell, is modulated at 850 Hz by a mechanical chopper, fed to a monomode optical fibre, focused and finally linearly polarised before impinging on the subwavelength structure mounted in the sample holder. The beam waist diameter and confocal parameter of the illuminating source are 300 μm and 33 cm, respectively. Throughout this series of measurements the laser power density was maintained $\sim 1\text{Wcm}^{-2}$. The sample holder itself is fixed to a precision x-y translator, and multiple structures, FIB-milled in a 2-D array on a single substrate, are successively positioned at the laser beam waist. The optical response of the structures is synchronously detected by a photodiode and registered on a laboratory computer as indicated in Fig. 3.

Acknowledgments

Support from the Ministère délégué à l’Enseignement supérieur et à la Recherche under the programme ACI-“Nanosciences-Nanotechnologies,” the Région Midi-Pyrénées [SFC/CR 02/22], and FASTNet [HPRN-CT-2002-00304] EU Research Training Network, is gratefully acknowledged as is support from the Caltech Kavli Nanoscience Institute and from the AFOSR under Plasmon MURI FA9550-04-1-0434. Discussions and technical assistance from P. Lalanne, R. Mathevet, F. Kalkum, G. Derose, A. Scherer, D. Pacifici, J. Dionne, R. Walters and H. Atwater are

also gratefully acknowledged.

-
- [1] Ebbesen, T. W., Lezec, H. J., Ghaemi, H. F., Thio, T., and Wolff, H. J. Extraordinary optical transmission through sub-wavelength hole arrays. *Nature* **391**, 667-669 (1998).
 - [2] Thio, T., Pellerin, K. M., Linke, R. A., Ebbesen, T. W., and Lezec, H. J. Enhanced light transmission through a single subwavelength aperture. *Opt. Lett.* **26**, 1972-1974 (2001).
 - [3] Ghaemi, H. F., Thio, T., Grupp, D. E., Ebbesen, T. W., and Lezec, H. J. Surface plasmons enhance optical transmission through subwavelength holes. *Phys. Rev. B* **58**, 6779-6782 (1998).
 - [4] Raether, H. *Surface Plasmons on Smooth and Rough Surfaces and on Gratings*, (Springer-Verlag, Berlin, 1988).
 - [5] Barnes, W. L., Dereux, A., and Ebbesen, T. W. Surface plasmon subwavelength optics. *Nature* **424**, 824-830 (2003).
 - [6] Treacy, M. J. Dynamical diffraction in metallic optical gratings. *Appl. Phys. Lett.* **75**, 606-608 (1999).
 - [7] Treacy, M. J. Dynamical diffraction explanation of the anomalous transmission of light through metallic gratings. *Phys. Rev. B* **66**, 195105-1-195105-11 (2002).
 - [8] Cao, Q., and Lalanne, P. Negative role of surface plasmons in the transmission of metallic gratings with very narrow slits. *Phys. Rev. Lett.* **88**, 057403-1-057403-4 (2002).
 - [9] García-Vidal, F. J., Lezec, H. J., Ebbesen, T. W., and Martin-Moreno, L. Multiple paths to enhance optical transmission through a single subwavelength slit. *Phys. Rev. Lett.* **90**, 213901-1-213901-4 (2003).
 - [10] Chang, S.-H., Gray, S. K., and Schatz, G. C., Surface plasmon generation and light transmission by isolated nanoholes and arrays of nanoholes in thin metal films. *Optics Express*, **13**, 3150-3165 (2005).
 - [11] Lezec, H. J. and Thio, T., Diffracted evanescent wave model for enhanced and suppressed optical transmission through subwavelength hole arrays. *Optics Express* **12**, 3629-3651 (2004).
 - [12] Mandel, L. and Wolf, E. *Optical Coherence and Quantum Optics*, pp. 109-120 (Cambridge University Press, Cambridge England, 1995).
 - [13] Kowarz, M. W. Homogeneous and evanescent contribution in scalar near-field diffraction. *Applied Optics* **34**, 3055-3063 (1995)
 - [14] Johnson, P. and Christy, R. Optical constants of the noble metals. *Phys. Rev. B* **11**, 1315-1323 (1975).
 - [15] Palik, E. (ed.) *Handbook of Optical Constants of Solids* (Academic Press, Inc., New York, 1985).
 - [16] Schouten, et al., Plasmon-Assisted Two-Slit Transmission: Young's Experiment Revisited. *Phys. Rev. Lett.* **94**, 053901-1-4 (2005).
 - [17] Lalanne, P., Hugonin, J. P., Rodier, J. C., Theory of Surface Plasmon Generation at Nanoslit Apertures. *Phys. Rev. Lett.* **95**, 263902-1-263902-4 (2005)
 - [18] Hibbins, A.P., Sambles, J.R., and Lawrence, C. R., Gratingless enhanced microwave transmission through a subwavelength aperture in a thick metal plate. *Appl. Phys. Lett.* **81**, 4661-4663 (2002).
 - [19] Abajo, F. J. García de, Light transmission through a single cylindrical hole in a metallic film. *Optics Express* **10**, 1475-1484 (2002).
 - [20] Popov, E., Nevière, M., Boyer, P., and Bonod, N., Light transmission through a subwavelength hole. *Optics Comm.* **255**, 338-348 (2005).
 - [21] Petit, R. *Electromagnetic Theory of Gratings*, pp. 136-144 (Springer-Verlag, Berlin, 1980)
 - [22] Mehan, N. and Mansingh, A., Study of tarnished films formed on silver by exposure to H₂S with the surface-plasmon resonance technique. *Appl. Optics* **39**, 5214-5220 (2000).